On the Performance of Non–Coherent Transmission Schemes with Equal–Gain Combining in Generalized K–Fading

Cindy Zhu, *Student Member, IEEE,* Jan Mietzner, *Member, IEEE,* and Robert Schober, *Fellow, IEEE*

***Abstract*— The generalized K–fading model, characterized by two parameters, k and m, is a very versatile model and was recently shown to accurately capture the effects of composite shadowing and multipath fading in wireless communication systems. Furthermore, it can be used to model cascade multipath fading, which is relevant in, e.g., mobile–to–mobile communication scenarios. In this paper, we derive closed–form expressions for the bit error probability of two non–coherent transmission schemes over L diversity branches being subject to generalized K–fading. Specifically, focus is on binary differential phase–shift keying (DPSK) and binary non–coherent frequency–shift keying (FSK) modulation with (post–detection) equal–gain combining at the receiver. We also discuss the extension of our results to M–ary modulation schemes. Considering both independent and correlated fading across the L branches, we derive expressions for the asymptotic diversity order, which reveal an interesting interplay between the two fading parameters k and m. Moreover, we show that the diversity order of the considered non–coherent transmission schemes is the same as in the case of a coherent transmission scheme. Finally, numerical performance results are presented, and our analytical results are corroborated by means of Monte–Carlo simulations.**

***Index Terms*— Fading channels, K–fading, shadowing, cascade fading, non–coherent transmission, diversity reception, performance analysis.**

I. Introduction

THE performance of wireless communication systems is largely governed by shadowing and multipath fading effects [1, Ch. 2]. While major obstacles between transmitter and receiver cause macroscopic fading effects, i.e., fluctuations in the *average* received signal–to–noise ratio (SNR), scatterers in the vicinity of transmitter and receiver entail microscopic fading effects, i.e., fluctuations in the *instantaneous* received SNR. Recently, the generalized K–fading model, which is characterized by two parameters, $k>0$ and $m>0$, was shown to accurately capture the effects of composite shadowing and multipath fading [2]. In particular, it comprises a large variety of channel conditions, ranging from severe shadowing (small values of k) to mild shadowing (large values of k) and from severe multipath fading (small values of m) to mild multipath fading (large values of m). The generalized K–fading model can also be employed to model cascade multipath fading, which occurs, e.g., in keyhole or in mobile–to–mobile communication scenarios [3], [4]. For the special case $k=m=1$, for example, the generalized K–fading model reduces to the double Rayleigh–fading model. By varying the fading parameters accordingly, more or less severe cascade multipath fading can be modeled. Finally, it is worth noting that the generalized K–fading model (also referred to as Gamma–Gamma fading model) occurs also in free–space optical (FSO) communications, where it is usually employed in order to model atmospheric turbulence conditions [5]–[8].

A favorable property of the generalized K–fading model is that it allows for a closed–form expression for the probability density function (PDF) of the instantaneous received SNR, which is in contrast to, e.g., competing composite shadowing/multipath fading models that are based on the lognormal PDF [2]. As a result, several analytical performance results for generalized K–fading and 'ordinary' K–fading channels ($m=1$) have been reported in the literature [9]–[18]. Moreover, analytical performance results for the special case of double Rayleigh fading were presented in [4], [19], [20].

Most of the papers mentioned above have focussed on coherent transmission schemes, which rely on the availability of accurate channel knowledge at the receiver side. In contrast to this, non–coherent transmission schemes eliminate the need for channel estimation at the receiver and are thus attractive for high–mobility and low–SNR scenarios as well as for low–cost receiver implementations. In this paper, we derive closed–form expressions for the bit error probability (BEP) of two non–coherent transmission schemes over L generalized K–fading branches with (post–detection) equal–gain combining (EGC) at the receiver. Specifically, focus is on binary differential phase–shift keying (DPSK) modulation with conventional differential detection at the receiver (i.e., based on two subsequent received symbols) and orthogonal binary frequency–shift keying (FSK) modulation with non–coherent detection at the receiver [21, Ch. 9.4]. We also discuss the extension of our results to M–ary modulation schemes. Concerning the generalized K–fading model we consider two scenarios. First, we focus on the case of independent fading across the L branches, which is, for example, relevant for cascade multipath fading. Given a rich–scattering radio environment (see [4] for examples), the assumption of uncorrelated diversity branches – created, e.g., by

Manuscript received February 5, 2009; revised September 2, 2009; accepted December 30, 2009. The associate editor coordinating the review of this paper and approving it for publication was Dr. Annamalai. This work was partly supported by a postdoctoral fellowship from the German Academic Exchange Service (DAAD). Part of this work was presented at the 2009 IEEE 70th Veh. Technol. Conf. (VTC2009-Fall), Anchorage, AK, USA, Sept. 2009.

Cindy Zhu, Robert Schober, and Jan Mietzner are with the Department of Electrical & Computer Engineering, The University of British Columbia, 2332 Main Mall, Vancouver, BC, Canada, V6T 1Z4 (e-mail: {yzhu,rschober}@ece.ubc.ca, jan.mietzner@ieee.org).

multiple receive antennas with sufficiently large antenna spacings – appears to be reasonable. Afterwards, we turn to the case of composite shadowing and multipath fading. Here, we consider the scenario where the shadowing part is fully correlated, whereas the multipath fading is independent and identically distributed (i.i.d.) across the L branches. Since shadowing represents a large–scale fading effect that is caused by buildings and other large–scale structures in the environment, it can typically be expected to affect all diversity branches simultaneously, while in a rich–scattering environment the multipath fading part can again be considered independent across links. For example, if the diversity branches are created by multiple receive antennas that are attached to the same wireless receiver unit, it can be expected that all diversity branches experience the same average SNR (full correlation), while the multipath fading is i.i.d., provided that the antenna spacings are sufficiently large (usually a couple of wavelengths).

For both the i.i.d. scenario and the scenario with fully correlated shadowing part, we present a high–SNR analysis and provide expressions for the resulting asymptotic diversity orders, which reveal an interesting interplay between the two fading parameters k and m. It is worth noting that the existing papers on non–coherent transmission schemes over (generalized) K–fading or double Rayleigh–fading links [4]–[11], [13] are all restricted to a single branch ($L\!=\!1$). In particular, for $L\!>\!1$ to the best of the authors' knowledge no closed–form expressions for the BEP and the asymptotic diversity order of the considered non–coherent transmission schemes in generalized K–fading have yet been presented in the literature. Also, there are no similar analyses for the competing composite lognormal shadowing/multipath fading model.

The remainder of this paper is organized as follows. In Section II, the generalized K–fading model is briefly recapitulated and certain moment–generating functions (MGFs) are derived, which are employed in the subsequent performance analysis. In Section III, the closed–form BEP expressions for binary DPSK/non–coherent FSK modulation over L generalized K–fading branches are presented. In Section IV, asymptotic performance results are reported. In particular, the diversity order of the non–coherent transmission schemes is determined and compared with that of a coherent transmission scheme. In Section V, we discuss the extension of our results to M–ary DPSK/non–coherent FSK modulation. Finally, numerical performance results are presented in Section VI, and conclusions are offered in Section VII.

II. The Generalized K–Fading Model

We start with a brief review of the PDF of the instantaneous received SNR for generalized K–fading. Subsequently, we derive certain MGFs for the case of cascade multipath fading and the case of composite shadowing/multipath fading.

A. PDF of the Instantaneous Received SNR

In order to derive the generalized K–distribution, consider first the case of composite shadowing and multipath fading. In this case, the generalized K–fading model describes a composite Gamma–shadowing/Nakagami–m fading process [2]. The PDF of the instantaneous SNR γ, conditioned on the average SNR $\bar{\gamma}$, is given by [22]

$$p_{\gamma|\bar{\gamma}}(\gamma|\bar{\gamma}) = \frac{m^m \gamma^{m-1}}{\Gamma(m)\bar{\gamma}^m}\, \exp\left(-\frac{m\gamma}{\bar{\gamma}}\right), \quad m\!>\!0, \;\; \gamma\!\geq\!0, \quad (1)$$

where $\Gamma(x)$ denotes the Gamma function. The average SNR $\bar{\gamma}$ itself is a random variable with PDF given by

$$p_{\bar{\gamma}}(\bar{\gamma}) = \frac{\bar{\gamma}^{k-1}}{\Gamma(k)\bar{\bar{\gamma}}^k}\, \exp\left(-\frac{\bar{\gamma}}{\bar{\bar{\gamma}}}\right), \quad k\!>\!0, \;\; \bar{\gamma}\!\geq\!0, \quad (2)$$

where $\bar{\bar{\gamma}} \triangleq \mathsf{E}\{\bar{\gamma}\}/k$ and $\mathsf{E}\{\cdot\}$ denotes statistical expectation.[1] There is a one–to–one mapping between the Gamma–shadowing parameter k and the mean μ_{dB} and the standard deviation σ_{dB} in dB occurring in the lognormal shadowing model [12]:

$$\mu_{\mathrm{dB}} = \frac{10}{\ln 10}\Big(\ln(\bar{\bar{\gamma}}) + \Psi(k)\Big) \;\; \mathrm{dB}, \quad (3)$$

$$\sigma_{\mathrm{dB}} = \frac{10}{\ln 10}\sqrt{\Psi'(k)} \;\; \mathrm{dB}, \quad (4)$$

where $\Psi(x) \triangleq \frac{\partial}{\partial x}\ln(\Gamma(x)) = (\frac{\partial}{\partial x}\Gamma(x))/\Gamma(x)$ denotes the Digamma function and $\Psi'(x) \triangleq \frac{\partial}{\partial x}\Psi(x)$ the Trigamma function. For example, for values of $k = 0.5,\, 1,\, 3$ one obtains standard deviations of $\sigma_{\mathrm{dB}} \approx 9.65$ dB (severe shadowing), $\sigma_{\mathrm{dB}}\!\approx\!5.56$ dB (moderate shadowing), and $\sigma_{\mathrm{dB}}\!\approx\!2.73$ dB (light shadowing), respectively.

Combining (1) and (2), the PDF of the instantaneous SNR γ results as [2]

$$p_\gamma(\gamma) = \frac{\eta^{\beta+1}}{\Gamma(k)\Gamma(m)2^\beta}\, \gamma^{\frac{\beta-1}{2}}\, K_\alpha(\eta\sqrt{\gamma}), \quad (5)$$

where $\eta\!\triangleq\!2\sqrt{m/\bar{\bar{\gamma}}}$, $\alpha\!\triangleq\!k\!-\!m$, $\beta\!\triangleq\!k\!+\!m\!-\!1$, and $K_\nu(x)$ denotes the modified Bessel function of the second kind and order ν. A widely–used measure to assess the severity of fading processes is the so–called amount of fading (AF) defined as $\mathrm{AF}\!\triangleq\!\frac{\mathsf{E}\{\gamma^2\}-(\mathsf{E}\{\gamma\})^2}{(\mathsf{E}\{\gamma\})^2}$. In the case of generalized K–fading, one obtains [12]

$$\mathrm{AF} = \frac{1}{k} + \frac{1}{m} + \frac{1}{km} > 0. \quad (6)$$

The value $\mathrm{AF}\!=\!1$ corresponds to Rayleigh fading, while values greater than one correspond to more severe fading and values smaller than one to less severe fading. Note that for $k, m\!\to\!\infty$, the generalized–K fading model tends to a non–fading additive white Gaussian noise (AWGN) channel model, as $\mathrm{AF}\!\to\!0$.

As mentioned earlier, the above PDF (5) for generalized K–fading can also be used in order to model cascade multipath

[1] We note that the principal form of the PDFs (1) and (2) is identical. This can be seen when replacing parameter $\bar{\bar{\gamma}}$ in (2) by a normalized parameter $\bar{\bar{\gamma}}' \triangleq k\bar{\bar{\gamma}}$. Consequently, the parameters k and m are, in principle, interchangeable. Since the definition of the constituent PDF (2) – with parameter $\bar{\bar{\gamma}}$ instead of $\bar{\bar{\gamma}}'$ – seems more consistent with the literature (see, e.g., [12]), we employ this definition throughout this paper, rather than choosing an identical form similar to (1) for both constituent PDFs (as, for example, done in [15]). In the context of the composite shadowing/multipath fading model, parameter k (related to (2)) is thus referred to as Gamma–shadowing parameter throughout this paper, and parameter m (related to (1)) is referred to as Nakagami–fading parameter. Moreover, parameter $\bar{\bar{\gamma}}$ is referred to as 'normalized average SNR' throughout this paper (since $\bar{\bar{\gamma}}\!=\!\mathsf{E}\{\bar{\gamma}\}/k\!=\!\bar{\bar{\gamma}}'/k$).

fading, where the instantaneous SNR γ results from a product $\gamma \triangleq \gamma_1\gamma_2$ of two statistically independent random variables γ_1 and γ_2 with PDFs of form (1) and (2), respectively. In this case, both k and m are related to Nakagami–fading processes. For example, for the special case $k=m=1$ one obtains the double Rayleigh–fading model [3], [4], where

$$p_\gamma(\gamma) = \frac{2}{\bar{\bar{\gamma}}}\, K_0\left(2\sqrt{\frac{\gamma}{\bar{\bar{\gamma}}}}\right) \tag{7}$$

($\bar{\bar{\gamma}} \triangleq \mathsf{E}\{\gamma\}$). By varying the parameters k and m accordingly, more or less severe cascade multipath fading can be modeled. In particular, for the special case $k=1$ and $m\neq 1$ one obtains a cascade multipath fading model composed of a Rayleigh fading process and a Nakagami–m fading process.

In the following, we consider transmission over L generalized K–fading branches and derive expressions for the MGF of the instantaneous sum SNR

$$\gamma_{\mathrm{t}} \triangleq \sum_{l=1}^{L} \gamma_l, \tag{8}$$

where γ_l denotes the instantaneous SNR associated with the lth branch ($l\in\{1,\ldots,L\}$). These expressions will later be utilized in Section IV to determine the diversity order of a coherent transmission scheme with maximum–ratio combining (MRC) at the receiver, and in Section V to extend our performance analysis for binary DPSK/non–coherent FSK modulation with EGC at the receiver (Section III) to the case of quaternary DPSK and M–ary non–coherent FSK modulation. We note that the derived MGF expressions could also be useful for other performance analyses (e.g., outage analysis) and are thus of general interest.

We start with the case of independent but not necessarily identically distributed (i.n.d.) fading across branches, which is relevant for the case of cascade multipath fading. Subsequently, we address the case of composite shadowing and multipath fading. Throughout this paper, we assume quasi–static channel conditions, i.e., the instantaneous SNRs of all fading branches remain constant over an entire block of data symbols and change randomly from one block to the next.

B. MGF of Sum SNR for the Case of I.N.D. Fading

Let $\bar{\bar{\gamma}}_l \triangleq \mathsf{E}\{\gamma_l\}/k$ denote the normalized average SNR associated with the lth branch ($l\in\{1,\ldots,L\}$). Since $\bar{\bar{\gamma}}_l$ will in general differ from one branch to the next, we define a reference level θ for all branches, according to $\theta \triangleq \min_{l\in\{1,\ldots,L\}}\{\bar{\bar{\gamma}}_l\}$. Thus, for each index $l \in \{1,\ldots,L\}$ the normalized average SNR $\bar{\bar{\gamma}}_l$ can be written as $\bar{\bar{\gamma}}_l \triangleq \delta_l \cdot \theta$ with constant $\delta_l \geq 1$. The reference SNR level θ will be later useful to study the behavior of the closed–form BEP expressions derived in Section III for high SNR values (i.e., $\theta \to \infty$), see Section IV.

In the following, the individual branches are assumed to be characterized by independent generalized K–fading, where for the lth branch the parameters of the PDF (5) are given by $\eta_l \triangleq 2\sqrt{m_l/\bar{\bar{\gamma}}_l}$, $\alpha_l \triangleq k_l - m_l$, and $\beta_l \triangleq k_l + m_l - 1$. The MGF of the instantaneous branch SNR γ_l, $\mathrm{M}_{\gamma_l}(x) \triangleq \mathsf{E}\{\mathrm{e}^{x\gamma_l}\}$, can be derived based on (5) by employing [§6.643, no. 3] from [23]. Using relation [§13.1.33] from [24, Ch. 13]

$$W_{\mu,\nu}(x) = \mathrm{e}^{-x/2}\, x^{\nu+1/2}\, U(1/2+\nu-\mu, 1+2\nu; x) \tag{9}$$

between the Whittaker function $W_{\mu,\nu}(x)$ and the confluent hypergeometric function of the second kind[2] $U(a,b;x)$, one obtains the following closed–form expression:

$$\mathrm{M}_{\gamma_l}(x) = \left(\frac{-m_l}{x\,\delta_l\,\theta}\right)^{k_l} U\left(k_l, 1+\alpha_l; \frac{-m_l}{x\,\delta_l\,\theta}\right). \tag{10}$$

We note that for numerical evaluation the representation [§13.1.3] from [24, Ch. 13] (see also [25])

$$\begin{aligned} U(a,b;x) &= \frac{\Gamma(1-b)}{\Gamma(a-b+1)}\, {}_1F_1(a,b;x) \\ &\quad + x^{1-b}\, \frac{\Gamma(b-1)}{\Gamma(a)}\, {}_1F_1(a-b+1, 2-b; x) \end{aligned} \tag{11}$$

of $U(a,b;x)$ in terms of the Kummer confluent hypergeometric function ${}_1F_1(a,b;x)$, which holds for all non–integer values of b, is sometimes preferable. It leads to the following expression for $\mathrm{M}_{\gamma_l}(x)$:[3]

$$\begin{aligned} \mathrm{M}_{\gamma_l}(x) &= \left(\frac{-m_l}{x\,\delta_l\,\theta}\right)^{k_l} \frac{\Gamma(-\alpha_l)}{\Gamma(m_l)}\, {}_1F_1\left(k_l, 1+\alpha_l; \frac{-m_l}{x\,\delta_l\,\theta}\right) \\ &\quad + \left(\frac{-m_l}{x\,\delta_l\,\theta}\right)^{m_l} \frac{\Gamma(\alpha_l)}{\Gamma(k_l)}\, {}_1F_1\left(m_l, 1-\alpha_l; \frac{-m_l}{x\,\delta_l\,\theta}\right) \end{aligned} \tag{12}$$

(α_l non–integer for all $l\in\{1,\ldots,L\}$). Due to the assumption of independent fading, the MGF of the instantaneous sum SNR γ_{t} according to (8), $\mathrm{M}_{\gamma_{\mathrm{t}}}(x) \triangleq \mathsf{E}\{\mathrm{e}^{x\gamma_{\mathrm{t}}}\}$, is given by

$$\mathrm{M}_{\gamma_{\mathrm{t}}}(x) = \prod_{l=1}^{L} \left(\frac{-m_l}{x\,\delta_l\,\theta}\right)^{k_l} U\left(k_l, 1+\alpha_l; \frac{-m_l}{x\,\delta_l\,\theta}\right). \tag{13}$$

In the case of i.i.d. fading, the above expression reduces to

$$\mathrm{M}_{\gamma_{\mathrm{t}}}(x) = \left(\frac{-m}{x\,\theta}\right)^{kL} \left[U\left(k, 1+\alpha; \frac{-m}{x\,\theta}\right)\right]^{L} \tag{14}$$

($k_1=\ldots=k_L\triangleq k$, $m_1=\ldots=m_L\triangleq m$, $\delta_1=\ldots=\delta_L\triangleq 1$).

C. MGF of Sum SNR for Correlated Composite Shadowing and Multipath Fading

In the case of composite shadowing and multipath fading, we assume that the shadowing part is fully correlated, whereas the multipath fading is i.i.d. across the L branches ($k_1=\ldots=k_L\triangleq k$, $m_1=\ldots=m_L\triangleq m$). Correspondingly, all

[2] $U(a,b;x)$ is also known as Kummer's function of the second kind or Tricomi's confluent hypergeometric function.

[3] Recently, for the special case $m=1$ an alternative expression for the MGF (10)/(12) was presented in [8], which is based on the two–parameter exponential integral function $\mathrm{Ei}(a,x)$. Similarly, for the special case $m=1$ an expression based on the incomplete Gamma function $\Gamma(a,x)$ was presented in [10]. Finally, for the general case an alternative expression for the MGF (10)/(12), which is based on the Whittaker function $W_{\lambda,\mu}(x)$, was presented in [13].

branches are characterized by the same average SNR, $\bar{\gamma}$, which itself is a random variable with PDF given by (2). Moreover, we have $\bar{\bar{\gamma}}_1 = \ldots = \bar{\bar{\gamma}}_L \triangleq \theta$. The joint PDF of the instantaneous branch SNRs γ_l ($l \in \{1, \ldots, L\}$), conditioned on the average SNR $\bar{\gamma}$, is given by

$$p_{\gamma_1,\ldots,\gamma_L|\bar{\gamma}}(\gamma_1, \ldots, \gamma_L|\bar{\gamma}) = \prod_{l=1}^{L} p_{\gamma_l|\bar{\gamma}}(\gamma_l|\bar{\gamma}), \tag{15}$$

due to the assumption of independent multipath fading across the L branches. Correspondingly, the conditional MGF of the instantaneous sum SNR $\gamma_{\rm t}$,

$$\mathrm{M}_{\gamma_{\rm t}|\bar{\gamma}}(x) \triangleq \int_0^\infty \mathrm{e}^{x\gamma_{\rm t}}\, p_{\gamma_{\rm t}|\bar{\gamma}}(\gamma_{\rm t}|\bar{\gamma})\, \mathrm{d}\gamma_{\rm t},$$

is given by

$$\mathrm{M}_{\gamma_{\rm t}|\bar{\gamma}}(x) = \prod_{l=1}^{L} \mathrm{M}_{\gamma_l|\bar{\gamma}}(x). \tag{16}$$

Based on (1) and [§3.381, no. 4] from [23], the conditional MGF of the instantaneous branch SNR γ_l,

$$\mathrm{M}_{\gamma_l|\bar{\gamma}}(x) \triangleq \int_0^\infty \mathrm{e}^{x\gamma_l}\, p_{\gamma_l|\bar{\gamma}}(\gamma_l|\bar{\gamma})\, \mathrm{d}\gamma_l,$$

can be calculated as

$$\mathrm{M}_{\gamma_l|\bar{\gamma}}(x) = \left(\frac{m}{m - x\,\bar{\gamma}}\right)^m, \quad \mathrm{Re}\{x\} < 0, \tag{17}$$

which is the well–known MGF for Nakagami–m fading [21, Ch. 2.2]. Based on (2), (16) and (17), the (unconditional) MGF of $\gamma_{\rm t}$ can be written as

$$\mathrm{M}_{\gamma_{\rm t}}(x) = \frac{1}{\Gamma(k)\,\theta^k} \int_0^\infty \frac{\bar{\gamma}^{k-1}}{\left(1 - \frac{x}{m}\bar{\gamma}\right)^{mL}} \cdot \mathrm{e}^{-\bar{\gamma}/\theta}\, \mathrm{d}\bar{\gamma}. \tag{18}$$

Assuming that m is a finite non–integer value[4] and employing [§3.383, no. 5] from [23], we find the following closed–form expression for the MGF of $\gamma_{\rm t}$:

$$\begin{aligned} \mathrm{M}_{\gamma_{\rm t}}(x) \;=\;& (k)_{-mL} \cdot (mL)_{1-k} \\ &\times \left[\left(\frac{-m}{x\,\theta}\right)^{mL} \frac{\Gamma(mL)\,\Gamma(1-mL)}{\Gamma(1-k)} \cdot L_{-mL}^{-\Delta_{k,m}}\left(\frac{-m}{x\,\theta}\right) \right. \\ &\left. - \left(\frac{-m}{x\,\theta}\right)^{k} \frac{\Gamma(k)\,\Gamma(1-k)}{\Gamma(1-mL)} \cdot L_{-k}^{\Delta_{k,m}}\left(\frac{-m}{x\,\theta}\right) \right], \\ & \theta < \infty, \quad \mathrm{Re}\{x\} < 0, \end{aligned} \tag{19}$$

where $(x)_\nu \triangleq \Gamma(x+\nu)/\Gamma(x)$ denotes the Pochhammer symbol and $L_a^b(x)$ the generalized Laguerre function. Moreover, we have used the identity $\Gamma(x)\Gamma(1-x) = \pi/\sin(\pi x)$ for the Gamma function and introduced the short–hand notation $\Delta_{k,m} \triangleq k - mL$. Note that (14) and (19) are quite different, even though they are based on identical parameters k, m, and θ. This is due to the fading correlations taken into account in (19), but not in (14). Finally, we note that similar to Section II-B, the MGF (19) can again be expressed in terms of the Kummer confluent hypergeometric function ${}_1F_1(a, b; x)$:

$$\begin{aligned} \mathrm{M}_{\gamma_{\rm t}}(x) \;=\;& \Gamma(\Delta_{k,m}) \\ &\times \left[\left(\frac{-m}{x\,\theta}\right)^{mL} \frac{1}{\Gamma(k)}\, {}_1F_1\!\left(mL, 1 - \Delta_{k,m}; \frac{-m}{x\,\theta}\right) \right. \\ & - \left(\frac{-m}{x\,\theta}\right)^{k} \frac{1}{\Gamma(mL)} \frac{\Gamma(1-\Delta_{k,m})}{\Gamma(1+\Delta_{k,m})} \\ &\left. \times\; {}_1F_1\!\left(k, 1 + \Delta_{k,m}; \frac{-m}{x\,\theta}\right) \right], \end{aligned} \tag{20}$$

where $\Delta_{k,m}$ must be non–integer.[5] In order to arrive at (20), we have used the relation [§13.6.9] from [24, Ch. 13] (see also [26])

$$L_a^b(x) = \frac{(b+1)_a}{\Gamma(a+1)}\, {}_1F_1(-a, b+1; x) \tag{21}$$

for non–integer values of b.

III. Performance Analysis for the Binary Case

In this section, we will derive closed–form BEP expressions for binary DPSK/non–coherent FSK modulation over L generalized K–fading branches with EGC at the receiver. As earlier, we start with the case of i.n.d. fading across branches. Subsequently, we turn to the case of composite shadowing and multipath fading with fully correlated shadowing part.

A. BEP for the Case of I.N.D. Fading

Considering binary DPSK/non–coherent FSK modulation over L branches with (post–detection) EGC at the receiver, the instantaneous EGC output SNR is given by $\gamma_{\rm t} \triangleq \sum_{l=1}^{L} \gamma_l$ [21, Ch. 9.4], where γ_l denotes the instantaneous SNR associated with the lth branch. For a fixed value of $\gamma_{\rm t}$, the BEP of binary DPSK/non–coherent FSK modulation over L branches with EGC at the receiver is given by [27, Ch. 14.4]

$$\begin{aligned} P_{\rm b}(\gamma_{\rm t}) \;&=\; \frac{1}{2^{2L-1}}\, \mathrm{e}^{-g\gamma_{\rm t}} \sum_{l=0}^{L-1} c_l\, (g\gamma_{\rm t})^l, \\ c_l \;&\triangleq\; \frac{1}{l!} \sum_{\kappa=0}^{L-1-l} \binom{2L-1}{\kappa}, \end{aligned} \tag{22}$$

where $g \triangleq 1$ for binary DPSK and $g \triangleq 1/2$ for binary non–coherent FSK modulation. In order to derive a closed–form expression for the average BEP $\bar{P}_{\rm b}(\theta) \triangleq \mathsf{E}_{\gamma_{\rm t}}\{P_{\rm b}(\gamma_{\rm t})\}$, we first note that the joint PDF of the instantaneous branch SNRs γ_l ($l \in \{1, \ldots, L\}$) is given by

$$p_{\gamma_1,\ldots,\gamma_L}(\gamma_1, \ldots, \gamma_L) = \prod_{l=1}^{L} p_{\gamma_l}(\gamma_l), \tag{23}$$

due to the assumption of independent fading across the L branches. Second, we define the index vector

$$\boldsymbol{\kappa} \triangleq [\kappa_1, \ldots, \kappa_L] \in \mathbb{N}_0^L$$

[4] As will be seen in Section VI, error probabilities for values $m \in \mathbb{N}$, where $\mathbb{N}$ denotes the set of all integers greater than zero, can typically be evaluated with a high accuracy by replacing m with a slightly different value $m \pm \epsilon \notin \mathbb{N}$, where $\epsilon > 0$ is a small perturbation value.

[5] A corresponding expression to (20) for the special case $m = 1$ can be found in [10].

and the index set

$$\mathbb{K}_l \triangleq \{\boldsymbol{\kappa} \in \mathbb{N}_0^L \,|\, \kappa_1 + \cdots + \kappa_L = l\},$$

where $\mathbb{N}_0$ denotes the set of all integers greater than or equal to zero. Finally, we note that the term γ_{t}^l can be expressed as [24, Ch. 24.1.2]

$$\gamma_{\mathrm{t}}^l = (\gamma_1 + \cdots + \gamma_L)^l = \sum_{\boldsymbol{\kappa} \in \mathbb{K}_l} \binom{l}{\boldsymbol{\kappa}} \gamma_1^{\kappa_1} \cdots \gamma_L^{\kappa_L}, \quad (24)$$

where $\binom{l}{\boldsymbol{\kappa}} \triangleq l!/(\kappa_1! \cdots \kappa_L!)$. Based on the above findings, the average BEP $\bar{P}_{\mathrm{b}}(\theta)$ can be written as

$$\bar{P}_{\mathrm{b}}(\theta) = \frac{1}{2^{2L-1}} \sum_{l=0}^{L-1} c_l \, g^l \sum_{\boldsymbol{\kappa} \in \mathbb{K}_l} \binom{l}{\boldsymbol{\kappa}} \times \left(\prod_{\lambda=1}^{L} \int_0^\infty \mathrm{e}^{-g\gamma_\lambda} \gamma_\lambda^{\kappa_\lambda} \, p_{\gamma_\lambda}(\gamma_\lambda) \, \mathrm{d}\gamma_\lambda \right). \quad (25)$$

Plugging in (5) for the PDFs $p_{\gamma_\lambda}(\gamma_\lambda)$, $\lambda \in \{1, ..., L\}$, and employing [§6.643, no. 3] from [23] in conjunction with (9), we obtain for the average BEP the following closed–form expression:

$$\bar{P}_{\mathrm{b}}(\theta) = \frac{1}{2^{2L-1}} \sum_{l=0}^{L-1} c_l \sum_{\boldsymbol{\kappa} \in \mathbb{K}_l} \binom{l}{\boldsymbol{\kappa}} \times \left(\prod_{\lambda=1}^{L} (k_\lambda)_{\kappa_\lambda} (m_\lambda)_{\kappa_\lambda} \left(\frac{m_\lambda}{g\,\delta_\lambda \theta} \right)^{k_\lambda} \times U\!\left(k_\lambda + \kappa_\lambda, 1 + \alpha_\lambda; \frac{m_\lambda}{g\,\delta_\lambda \theta} \right) \right). \quad (26)$$

For the special case of i.i.d. fading, where $k_1 = ... = k_L \triangleq k$, $m_1 = ... = m_L \triangleq m$, $\alpha \triangleq k - m$, and $\delta_1 = ... = \delta_L = 1$, (26) simplifies to

$$\bar{P}_{\mathrm{b}}(\theta) = \frac{1}{2^{2L-1}} \left(\frac{m}{g\,\theta} \right)^{kL} \sum_{l=0}^{L-1} c_l \sum_{\boldsymbol{\kappa} \in \mathbb{K}_l} \binom{l}{\boldsymbol{\kappa}} \times \left(\prod_{\lambda=1}^{L} (k)_{\kappa_\lambda} (m)_{\kappa_\lambda} \cdot U\!\left(k + \kappa_\lambda, 1 + \alpha; \frac{m}{g\,\theta} \right) \right). \quad (27)$$

Finally, for the special case $L = 1$, (22) reduces to $P_{\mathrm{b}}(\gamma_{\mathrm{t}}) = P_{\mathrm{b}}(\gamma_1) = \frac{1}{2} \, \mathrm{e}^{-g\gamma_1}$, and $\bar{P}_{\mathrm{b}}(\theta)$ can be evaluated as

$$\bar{P}_{\mathrm{b}}(\theta) = \frac{1}{2} \left(\frac{m}{g\,\theta} \right)^k U\!\left(k, 1 + \alpha; \frac{m}{g\,\theta} \right). \quad (28)$$

For comparison, in the case of i.i.d. Rayleigh fading the average BEP $\bar{P}_{\mathrm{b}}(\theta)$ is given by [27, Ch. 14.4]

$$\bar{P}_{\mathrm{b}}(\theta) = \frac{1}{2^{2L-1}(L-1)!\,(1+g\,\theta)^L} \sum_{l=0}^{L-1} c_l \, (L-1+l)! \left(\frac{g\,\theta}{1+g\,\theta} \right)^l, \quad (29)$$

and we have

$$\bar{P}_{\mathrm{b}}(\theta) = \frac{1}{2(1+g\,\theta)} \quad (30)$$

for the special case $L = 1$.

B. BEP for Correlated Composite Shadowing and Multipath Fading

In the case of composite shadowing and multipath fading, we again assume that the shadowing part is fully correlated, whereas the multipath fading is i.i.d. across the L branches. In order to arrive at a closed–form expression for the average BEP $\bar{P}_{\mathrm{b}}(\theta)$, we first average (22) over the instantaneous branch SNRs γ_l, while conditioning on $\bar{\gamma}$. In the final step, the resulting conditional BEP, denoted as $\bar{P}_{\mathrm{b}}(\bar{\gamma})$, is then averaged over $\bar{\gamma}$.

Similar to (25), the conditional BEP $\bar{P}_{\mathrm{b}}(\bar{\gamma})$ can be written as

$$\bar{P}_{\mathrm{b}}(\bar{\gamma}) = \frac{1}{2^{2L-1}} \sum_{l=0}^{L-1} c_l \, g^l \sum_{\boldsymbol{\kappa} \in \mathbb{K}_l} \binom{l}{\boldsymbol{\kappa}} \times \left(\prod_{\lambda=1}^{L} \int_0^\infty \mathrm{e}^{-g\gamma_\lambda} \gamma_\lambda^{\kappa_\lambda} \, p_{\gamma_\lambda|\bar{\gamma}}(\gamma_\lambda|\bar{\gamma}) \, \mathrm{d}\gamma_\lambda \right), \quad (31)$$

where we have used that the joint PDF $p_{\gamma_1,...,\gamma_L|\bar{\gamma}}(\gamma_1, ..., \gamma_L|\bar{\gamma})$, conditioned on the average SNR $\bar{\gamma}$, can be written as the product of the conditional PDFs $p_{\gamma_l|\bar{\gamma}}(\gamma_l|\bar{\gamma})$ of the instantaneous branch SNRs γ_l ($l \in \{1, ..., L\}$), cf. (15). Plugging in (1) for the conditional PDFs $p_{\gamma_l|\bar{\gamma}}(\gamma_l|\bar{\gamma})$ and employing [§3.381, no. 4] from [23], we find the following expression for $\bar{P}_{\mathrm{b}}(\bar{\gamma})$:

$$\bar{P}_{\mathrm{b}}(\bar{\gamma}) = \frac{1}{2^{2L-1}} \left(\frac{m^m}{\Gamma(m)} \right)^L \sum_{l=0}^{L-1} c_l \, g^l \sum_{\boldsymbol{\kappa} \in \mathbb{K}_l} \binom{l}{\boldsymbol{\kappa}} \times \left(\prod_{\lambda=1}^{L} \Gamma(m + \kappa_\lambda) \frac{\bar{\gamma}^{\kappa_\lambda}}{(g\bar{\gamma} + m)^{m + \kappa_\lambda}} \right) \quad (32)$$

($m_1 = ... = m_L \triangleq m$). Based on the PDF (2) of the average SNR $\bar{\gamma}$, the average BEP $\bar{P}_{\mathrm{b}}(\theta) \triangleq \mathsf{E}_{\bar{\gamma}}\{\bar{P}_{\mathrm{b}}(\bar{\gamma})\}$ can be written as

$$\bar{P}_{\mathrm{b}}(\theta) = \frac{1}{2^{2L-1}} \frac{1}{\Gamma(k)(\Gamma(m))^L \, \theta^k} \sum_{l=0}^{L-1} c_l \, g^l \sum_{\boldsymbol{\kappa} \in \mathbb{K}_l} \binom{l}{\boldsymbol{\kappa}} \times \frac{\prod_{\lambda=1}^{L} \Gamma(m + \kappa_\lambda)}{m^l} \int_0^\infty \frac{\bar{\gamma}^{k+l-1} \cdot \mathrm{e}^{-\bar{\gamma}/\theta}}{(\frac{g}{m}\bar{\gamma} + 1)^{mL+l}} \, \mathrm{d}\bar{\gamma}. \quad (33)$$

Employing [§3.383, no. 5] from [23] and assuming that (i) m is a finite non–integer value and (ii) $k \neq mL$, we find the following closed–form expression for the average BEP $\bar{P}_{\mathrm{b}}(\theta)$:

$$\bar{P}_{\mathrm{b}}(\theta) = \frac{1}{2^{2L-1}} \frac{1}{\Gamma(k)} \frac{\pi}{\sin(\pi \Delta_{k,m})} \sum_{l=0}^{L-1} c_l \times \left[\sum_{\boldsymbol{\kappa} \in \mathbb{K}_l} \binom{l}{\boldsymbol{\kappa}} \left(\prod_{\lambda=1}^{L} (m)_{\kappa_\lambda} \right) \right] \times \left[\left(\frac{m}{g\,\theta} \right)^{mL} \frac{\Gamma(1 - \varphi_{m,l})}{\Gamma(1 - \psi_{k,l})} L_{-\varphi_{m,l}}^{-\Delta_{k,m}}\!\left(\frac{m}{g\,\theta} \right) - \left(\frac{m}{g\,\theta} \right)^{k} \frac{\sin(\pi \varphi_{m,l})}{\sin(\pi \psi_{k,l})} L_{-\psi_{k,l}}^{\Delta_{k,m}}\!\left(\frac{m}{g\,\theta} \right) \right], \quad (34)$$

where we have introduced the short–hand notations $\psi_{k,l} \triangleq k + l$ and $\varphi_{m,l} \triangleq mL + l$; thus, $\Delta_{k,m} = \psi_{k,l} - \varphi_{m,l}$. Note again that

(27) and (34) are quite different, due to the fading correlations taken into account in (34). This will also become obvious in the numerical results presented in Section VI.

IV. Asymptotic Analysis and Diversity Order

The closed–form BEP expressions (26) and (34) are relatively easy to evaluate (using, e.g., mathematical programs such as Maple© or Mathematica©), but involve some non–standard functions. Correspondingly, the primary behavior of the resulting BEP curves is not obvious. In this section, we will therefore study the behavior of (26) and (34) for high SNR values ($\theta \to \infty$). In particular, we derive expressions for the resulting (asymptotic) diversity order[6]

$$\begin{aligned} d &\triangleq \lim_{\theta\to\infty} d(\theta), \\ d(\theta) &\triangleq -\frac{\partial \log(\bar{P}_{\mathrm{b}}(\theta))}{\partial \log(\theta)}. \end{aligned} \tag{35}$$

In particular, we show that the diversity order of binary DPSK/ non–coherent FSK modulation is, in fact, the same as that in the case of a coherent transmission scheme.

A. The Case of Independent Fading

For the ease of exposition, we focus on the case of i.i.d. fading here, i.e., $\bar{\bar{\gamma}}_1 = \ldots = \bar{\bar{\gamma}}_L = \theta$, $m_1 = \ldots = m_L \triangleq m$, and $k_1 = \ldots = k_L \triangleq k$. An extension to the case of i.n.d. fading is, however, straightforward. In the following, we derive approximate expressions for the average BEP (27), by employing corresponding approximations of the confluent hypergeometric function $U(a, b; x)$.

Consider first the case where the two fading parameters k and m are different, i.e., $\alpha = k - m \neq 0$. For simplicity, we assume that α is a non–integer value. For $x \to 0$ and non–integer values of b, the confluent hypergeometric function $U(a, b; x)$ can be approximated using [§13.5.2] from [24, Ch. 13] (see also [28]):

$$U(a,b;x) \doteq \frac{\Gamma(1-b)}{\Gamma(1-b+a)} + \frac{\Gamma(b-1)}{\Gamma(a)}\, x^{1-b}, \tag{36}$$

where $\doteq$ denotes asymptotic equality. For $\theta \to \infty$ and non–integer values of α, we thus find

$$\begin{aligned} &\left(\frac{m}{g\,\theta}\right)^{k} U\left(k+\kappa_\lambda, 1+\alpha; \frac{m}{g\,\theta}\right) \\ &\quad\doteq \frac{\Gamma(-\alpha)}{\Gamma(m+\kappa_\lambda)}\left(\frac{m}{g\,\theta}\right)^{k} + \frac{\Gamma(\alpha)}{\Gamma(k+\kappa_\lambda)}\left(\frac{m}{g\,\theta}\right)^{m} \\ &\quad\doteq \frac{\Gamma(|\alpha|)}{\Gamma(\xi_2+\kappa_\lambda)}\left(\frac{m}{g\,\theta}\right)^{\xi_1}, \end{aligned} \tag{37}$$

where $\xi_1 \triangleq \min\{k, m\}$ and $\xi_2 \triangleq \max\{k, m\}$. Thus, the average BEP (27) can be approximated as

$$\begin{aligned} \bar{P}_{\mathrm{b}}(\theta) &\doteq \frac{1}{2^{2L-1}}\left(\frac{m}{g\,\theta}\right)^{\xi_1 L}\left(\frac{\Gamma(|\alpha|)}{\Gamma(\xi_2)}\right)^{L} \\ &\quad\times \sum_{l=0}^{L-1} c_l \sum_{\boldsymbol{\kappa}\in\mathbb{K}_l}\binom{l}{\boldsymbol{\kappa}}\left(\prod_{\lambda=1}^{L}(\xi_1)_{\kappa_\lambda}\right). \end{aligned} \tag{38}$$

From (38) we find

$$d = \xi_1 L = \min\{k, m\}\cdot L. \tag{39}$$

Note that due to the restrictions on (38), (39) holds only for non–integer values of α. Interestingly, the smaller of the two fading parameters, k and m, limits the asymptotic diversity order. For example, in the case of cascade Rayleigh/Nakagami–m fading with $k=1$ and $m \geq 1$, the asymptotic diversity order is always given by $d = L$, just as in the case of pure Rayleigh fading, where [27, Ch. 14.4]

$$\bar{P}_{\mathrm{b}}(\theta) \doteq \left(\frac{1}{2g\,\theta}\right)^{L}\binom{2L-1}{L}. \tag{40}$$

Next, consider the case $\alpha = 0$, i.e., $k = m$. For $x \to 0$ and $b = 1$, the confluent hypergeometric function $U(a, b; x)$ can be approximated according to [§13.5.9] from [24, Ch. 13] as

$$U(a,b;x) \doteq -\frac{1}{\Gamma(a)}\big(\ln(x) + \Psi(a) + 2\gamma'\big), \tag{41}$$

where $\Psi(x)$ again denotes the Digamma function, and γ' the Euler–Mascheroni constant. For $\theta \to \infty$ and $\alpha = 0$, we thus find

$$\begin{aligned} &\left(\frac{m}{g\,\theta}\right)^{k} U\left(k+\kappa_\lambda, 1+\alpha; \frac{m}{g\,\theta}\right) \\ &\quad\doteq -\frac{1}{\Gamma(k+\kappa_\lambda)}\left[\left(\frac{m}{g\,\theta}\right)^{k}\ln\left(\frac{m}{g\,\theta}\right) + \left(\Psi(k+\kappa_\lambda)+2\gamma'\right)\left(\frac{m}{g\,\theta}\right)^{k}\right] \\ &\quad\doteq -\frac{1}{\Gamma(k+\kappa_\lambda)}\left(\frac{m}{g\,\theta}\right)^{k}\ln\left(\frac{m}{g\,\theta}\right), \end{aligned} \tag{42}$$

i.e., the average BEP (27) can be approximated as

$$\begin{aligned} \bar{P}_{\mathrm{b}}(\theta) &\doteq \frac{1}{2^{2L-1}}\left[-\left(\frac{m}{g\,\theta}\right)^{k}\ln\left(\frac{m}{g\,\theta}\right)\right]^{L} \\ &\quad\times \sum_{l=0}^{L-1} c_l \sum_{\boldsymbol{\kappa}\in\mathbb{K}_l}\binom{l}{\boldsymbol{\kappa}}\left(\prod_{\lambda=1}^{L}\frac{(k)_{\kappa_\lambda}(m)_{\kappa_\lambda}}{\Gamma(k+\kappa_\lambda)}\right). \end{aligned} \tag{43}$$

Correspondingly, we find

$$d(\theta) = \left(k - \frac{1}{\ln(\theta)}\right)L = \left(m - \frac{1}{\ln(\theta)}\right)L, \tag{44}$$

i.e., the asymptotic diversity order is given by

$$d = kL = mL. \tag{45}$$

This result is in accordance with [4], where the diversity order of various coherent modulation schemes was determined for the special case of a single branch ($L=1$) being subject to double Rayleigh fading ($k=m=1$). Moreover, note that (45) is also in accordance with (39).

[6] The (asymptotic) diversity order is the negative slope of the BEP curve for high SNR values on a log–log scale. It has been shown to be a useful measure for characterizing the principal behavior of digital transmission schemes over various fading channels [27, Ch. 14.4].

Finally, we compare the above results for binary DPSK/non–coherent FSK modulation with the asymptotic diversity order obtained in the case of a coherent transmission scheme. As an example, we consider binary PSK over L i.i.d. generalized K–fading links with MRC at the receiver. The corresponding average BEP can be determined via the following finite–range integral [29]:

$$\bar{P}_{\mathrm{b}}(\theta) = \frac{1}{\pi}\int_0^{\pi/2} \mathrm{M}_{\gamma_{\mathrm{t}}}\left(-\frac{1}{\sin^2(\phi)}\right)\mathrm{d}\phi, \tag{46}$$

where the MGF $\mathrm{M}_{\gamma_{\mathrm{t}}}(x)$ of the instantaneous MRC output SNR $\gamma_{\mathrm{t}} = \sum_{l=1}^{L}\gamma_l$ is given by (14).[7] As earlier, we assume for simplicity that α is a non–integer value. Based on (36) and employing [§3.621, no. 1] from [23], the average BEP (46) for high SNR values $\theta \to \infty$ can be approximated as

$$\bar{P}_{\mathrm{b}}(\theta) \doteq \frac{1}{2\pi}\left(\frac{\Gamma(|\alpha|)}{\Gamma(\xi_2)}\right)^{L}\left(\frac{4m}{\theta}\right)^{\xi_1 L} B\big(\xi_1 L{+}1/2, \xi_1 L{+}1/2\big), \tag{47}$$

where $B(x,y)$ denotes the Beta function. Correspondingly, the diversity order of binary PSK modulation over L i.i.d. generalized K–fading links with MRC at the receiver is given by

$$d = \xi_1 L = \min\{k, m\}\cdot L \tag{48}$$

(α non–integer), just as in the case of the considered non–coherent transmission schemes, cf. (39).

B. Correlated Composite Shadowing and Multipath Fading

Next, we derive an approximate expression for the average BEP (34) for high SNR values $\theta \to \infty$, by employing a corresponding approximation of the generalized Laguerre function $L_a^b(x)$. For $x \to 0$, the generalized Laguerre function $L_a^b(x)$ can be approximated as [30, Ch. 13.2] (see also [31])

$$L_a^b(x) \doteq \frac{(b{+}1)_a}{\Gamma(a{+}1)}. \tag{49}$$

For $\theta \to \infty$, the average BEP (34) can thus be approximated as

$$\begin{aligned}\bar{P}_{\mathrm{b}}(\theta) \;\doteq\; & \frac{1}{2^{2L-1}}\,\frac{\mathrm{sign}(\Delta_{k,m})}{\Gamma(k)}\,\frac{\pi}{\sin(\pi\Delta_{k,m})}\left(\frac{m}{g\,\theta}\right)^{\zeta_1}\sum_{l=0}^{L-1} c_l\,\Xi_l \\ & \times\left[\sum_{\boldsymbol{\kappa}\in\mathbb{K}_l}\binom{l}{\boldsymbol{\kappa}}\left(\prod_{\lambda=1}^{L}(m)_{\kappa_\lambda}\right)\right]\frac{(1-|\Delta_{k,m}|)_{-\zeta_1-l}}{\Gamma(1-\psi_{k,l})},\end{aligned} \tag{50}$$

where $\zeta_1 \triangleq \min\{k, mL\}$, $\mathrm{sign}(x)$ denotes the sign function (i.e., $\mathrm{sign}(x){=}{+}1$ for all $x \geq 0$ and $\mathrm{sign}(x){=}{-}1$ otherwise), and[8]

$$\Xi_l \triangleq \begin{cases} \sin(\pi\varphi_{m,l})/\sin(\pi\psi_{k,l}) & \text{for } k < mL \\ 1 & \text{for } k > mL \end{cases}. \tag{51}$$

[7]It is worth noting that a further evaluation of (46) based on (14) – or (19) for that matter – seems difficult.

[8]As earlier, we assume that $k \neq mL$, since otherwise (34) is not valid. However, it turns out that (50) yields nearly identical results for $k = mL + \epsilon$ and $k = mL - \epsilon$, if ϵ is chosen sufficiently small.

Correspondingly, the asymptotic diversity order in the case of correlated composite shadowing and multipath fading is obtained as

$$d = \zeta_1 = \min\{k, mL\}. \tag{52}$$

This result reveals an interesting interplay between macroscopic diversity due to shadowing effects and microscopic diversity due to multipath fading: the asymptotic diversity order is always limited by either the shadowing effect ($k < mL$) or the multipath fading ($mL < k$), depending on which one of the two fading effects is more severe.

In order to arrive at (50), we have utilized that for $\theta \to \infty$ only one of the two $L_a^b(x)$–terms in (34) dominates, namely the one which is associated with the term $(\frac{m}{g\,\theta})^{\zeta_1}$. Correspondingly, if $k \approx mL$ the convergence of the asymptotic solution (50) to the exact expression (34) can be expected to be rather slow, since the dominant term will only emerge for very large values of θ. However, if k and mL are sufficiently different, the convergence of (50) is typically quite fast, as will be seen from the numerical performance results presented in Section VI.

In order to compare the asymptotic diversity order (52) for binary DPSK/non–coherent FSK modulation with that in the case of binary PSK modulation, we first note that (46) is valid for arbitrary fading correlations (if an expression for the MGF $\mathrm{M}_{\gamma_{\mathrm{t}}}(x)$ of the instantaneous MRC output SNR γ_{t} is available). In the case of correlated composite shadowing and multipath fading, the MGF $\mathrm{M}_{\gamma_{\mathrm{t}}}(x)$ is given by (19). Based on (49) and employing [§3.621, no. 1] from [23], the average BEP (46) for $\theta \to \infty$ can be approximated as

$$\begin{aligned}\bar{P}_{\mathrm{b}}(\theta) \;\doteq\; & \frac{\mathrm{sign}(\Delta_{k,m})\;(k)_{-mL}\cdot(mL)_{1-k}}{2\pi} \\ & \times\frac{\Gamma(\zeta_1)\;(1-|\Delta_{k,m}|)_{-\zeta_1}}{\Gamma(1-\zeta_2)}\left(\frac{4m}{\theta}\right)^{\zeta_1} \\ & \times B\big(\zeta_1{+}1/2, \zeta_1{+}1/2\big),\end{aligned} \tag{53}$$

where $\zeta_2 \triangleq \max\{k, mL\}$. Correspondingly, the diversity order of binary PSK modulation over L correlated composite shadowing/multipath fading links with MRC at the receiver is given by

$$d = \zeta_1 = \min\{k, mL\}, \tag{54}$$

just as in the case of the non–coherent schemes, cf. (52).

V. Extensions to M–ary Modulation Schemes

The closed–form expressions (13) and (19) for the MGF of the instantaneous sum SNR γ_{t} in the case of i.n.d. fading and correlated composite shadowing/multipath fading, respectively, can be utilized to extend our performance analysis in Section III to the case of non–binary transmission schemes. As an example, we will focus on the average BEP of quaternary DPSK modulation with Gray mapping, the average BEP of M–ary orthogonal FSK modulation, and the average symbol error probability (SEP) of coherent M–ary PSK modulation.

A. Error Probability for the Case of I.N.D. Fading

In the case of i.n.d. fading, the average BEP of quaternary DPSK modulation with Gray mapping over L branches with (post–detection) EGC at the receiver is given by [21, Ch. 9.4]

$$\bar{P}_{\mathrm{b}}(\theta) = \frac{1}{\pi\, 2^{2L}} \int_{-\pi}^{\pi} \frac{f(L,\rho;\phi)}{1+2\rho\sin(\phi)+\rho^2} \times \prod_{l=1}^{L} \mathrm{M}_{\gamma_l}\left(-2-\sqrt{2}\sin(\phi)\right)\,\mathrm{d}\phi, \quad (55)$$

where

$$f(L,\rho;\phi) \triangleq \sum_{l=1}^{L} c'_l \cdot \Big[a_1(\rho)\cdot\cos\left((l-1)(\phi+\pi/2)\right) - a_2(\rho)\cdot\cos\left(l(\phi+\pi/2)\right)\Big], \quad (56)$$

$$c'_l \triangleq \binom{2L-1}{L-l}, \quad (57)$$

$$a_1(\rho) \triangleq \rho^{-l+1} - \rho^{l+1}, \quad (58)$$

$$a_2(\rho) \triangleq \rho^{-l+2} - \rho^{l}, \quad (59)$$

$$\rho \triangleq \sqrt{\frac{2-\sqrt{2}}{2+\sqrt{2}}}, \quad (60)$$

and $\mathrm{M}_{\gamma_l}(x)$ is given by (10). Thus, the average BEP (55) for the case of i.n.d. generalized K–fading can be evaluated numerically via a single finite–range integral over known functions. Similarly, the average BEP for M–ary orthogonal FSK over L branches with non–coherent detection and EGC at the receiver can be evaluated numerically based on the single finite–range integral expression (9.130) in [21, Ch. 9.4], which again depends on the product of the MGFs $\mathrm{M}_{\gamma_l}(x)$, $l\in\{1,...,L\}$. Finally, the average SEP for coherent M–ary PSK modulation over L branches with MRC at the receiver can be calculated via the finite–range integral[9] [29]

$$\bar{P}_{\mathrm{s}}(\theta) = \frac{1}{\pi}\int_0^{(M-1)\pi/M} \prod_{l=1}^{L} \mathrm{M}_{\gamma_l}\left(-\frac{\sin^2(\pi/M)}{\sin^2(\phi)}\right)\mathrm{d}\phi. \quad (61)$$

For the special case $L=1$, there is also a finite–range integral expression for the average SEP of M–ary DPSK modulation [21, Ch. 8.2.5]:

$$\bar{P}_{\mathrm{s}}(\theta) = \frac{1}{\pi}\int_0^{(M-1)\pi/M} \mathrm{M}_{\gamma_1}\left(-\frac{\sin^2(\pi/M)}{1+\sqrt{1-\sin^2(\pi/M)}\cos(\phi)}\right)\mathrm{d}\phi. \quad (62)$$

Next, we consider the case of correlated composite shadowing and multipath fading.

B. Error Probability for Correlated Composite Shadowing and Multipath Fading

As shown in the Appendix, (55) is also valid for the case of fully correlated shadowing/i.i.d. multipath fading. Thus, we have

$$\bar{P}_{\mathrm{b}}(\theta) = \frac{1}{\pi\, 2^{2L}} \int_{-\pi}^{\pi} \frac{f(L,\rho;\phi)}{1+2\rho\sin(\phi)+\rho^2} \times \mathrm{M}_{\gamma_{\mathrm{t}}}\left(-2-\sqrt{2}\sin(\phi)\right)\,\mathrm{d}\phi, \quad (63)$$

[9] Similar expressions can also be stated for M–ary amplitude–shift–keying (ASK) modulation and M–ary quadrature–amplitude modulation (QAM) [29].

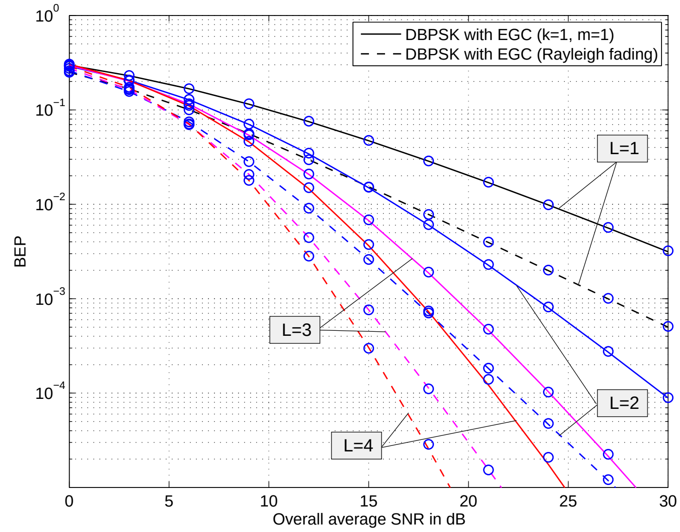

Fig. 1. Average BEP $\bar{P}_{\mathrm{b}}(\theta)$ versus (normalized) overall average SNR $L\,\theta$ in dB for the case of i.i.d. double Rayleigh fading ($k=1$, $m=1$). Solid lines represent analytical results for binary DPSK (DBPSK) modulation with EGC at the receiver evaluated based on (27)/(28) using the values $k=1.01$ and $m=0.99$. Dashed lines represent corresponding analytical results for the case of i.i.d. Rayleigh fading evaluated based on (29)/(30). Corresponding simulation results for Rayleigh fading and double Rayleigh fading ($k=1$, $m=1$) are indicated by markers 'o'.

where $\mathrm{M}_{\gamma_{\mathrm{t}}}(x)$ is given by (19).[10] Similarly, (61) again holds for arbitrary fading correlations, i.e., we have

$$\bar{P}_{\mathrm{s}}(\theta) = \frac{1}{\pi}\int_0^{(M-1)\pi/M} \mathrm{M}_{\gamma_{\mathrm{t}}}\left(-\frac{\sin^2(\pi/M)}{\sin^2(\phi)}\right)\mathrm{d}\phi. \quad (64)$$

Based on (19), the average SEP (64) for correlated composite shadowing and multipath fading can thus be evaluated numerically via a single finite–range integral over known functions.

VI. Numerical Performance Results

In the following, numerical performance results are presented, which illustrate our findings in Sections III–V. In particular, we will present Monte–Carlo simulation results, so as to corroborate our analytical performance results.

A. The Case of Independent Fading

In the following, we investigate the BEP performance of binary DPSK modulation over L independent generalized K–fading branches with EGC at the receiver (cf. Section III-A and Section IV-A). As an example, we focus on the case of i.i.d. cascade Rayleigh/Nakagami–m fading with $k=1$ and $m\geq 1$.

Fig. 1 shows the average BEP $\bar{P}_{\mathrm{b}}(\theta)$ for binary DPSK versus the normalized overall average received SNR $L\,\theta$ in dB for the case of i.i.d. double Rayleigh fading ($k=1$, $m=1$). The solid lines represent analytical results for $L\in\{1,...,4\}$ evaluated based on (27) and (28) using the values $k=1.01$ and $m=0.99$.[11] Corresponding simulation results (for $k=1$ and

[10] Note that (63) is not valid for arbitrary fading correlations.

[11] The confluent hypergeometric function $U(a,b;x)$ occurring in (27) and (28) was evaluated based on (11). While (27) and (28) themselves hold for any value of k and m, the alternative representation (11) of $U(a,b;x)$ can only be employed for non–integer values of $\alpha=k-m$. Hence, we have used values for k and m that slightly deviate from integer values.

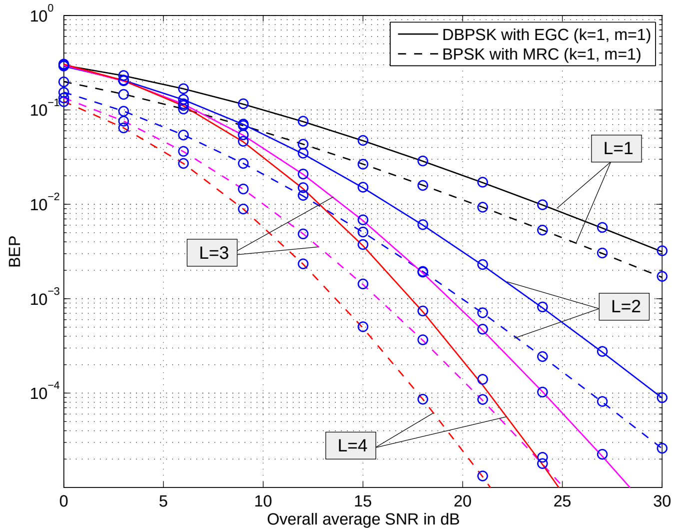

Fig. 2. Average BEP $\bar{P}_{\mathrm{b}}(\theta)$ versus (normalized) overall average SNR $L\,\theta$ in dB for the case of i.i.d. double Rayleigh fading ($k = 1$, $m = 1$). Solid lines represent analytical results for DBPSK modulation with EGC at the receiver evaluated based on (27)/(28) using the values $k=1.01$ and $m=0.99$. Dashed lines represent corresponding analytical results for coherent binary PSK modulation (BPSK) with MRC at the receiver evaluated based on (14), (46) using numerical integration. Corresponding simulation results for $k = 1$ and $m = 1$ are indicated by markers 'o' (both for DPSK and PSK modulation).

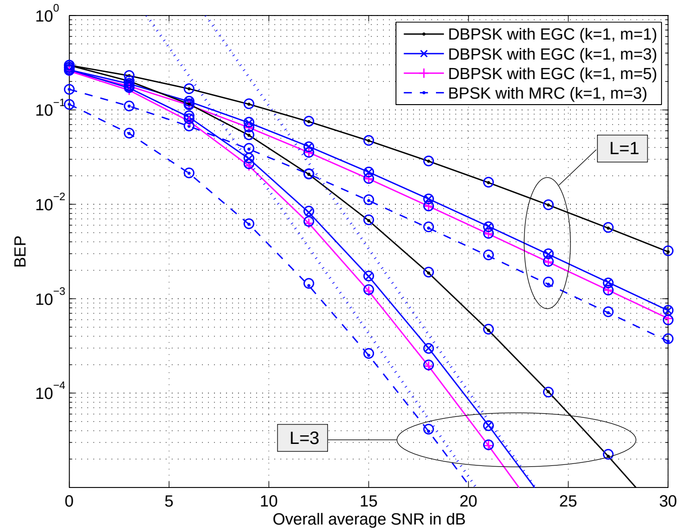

Fig. 3. Average BEP $\bar{P}_{\mathrm{b}}(\theta)$ versus (normalized) overall average SNR $L\,\theta$ in dB for different cases of cascade fading ($k=1$ and $m \in \{1,\ 3,\ 5\}$). Solid lines represent analytical results for DBPSK modulation with EGC at the receiver evaluated based on (27)/(28) using the values $k=1.01$ and $m \in \{0.99,\ 2.99,\ 4.99\}$, respectively. Dashed lines represent corresponding analytical results for coherent BPSK modulation with MRC at the receiver evaluated based on (14), (46) using numerical integration. Corresponding simulation results for $k = 1$ and $m \in \{1,\ 3,\ 5\}$ are indicated by markers 'o' (both for DPSK and PSK modulation). The dotted lines represent asymptotic BEP curves for the case $m=3$, $L=3$ evaluated based on (38) for DPSK modulation and based on (47) for PSK modulation.

$m=1$), obtained by Monte–Carlo simulations over a large number of independent channel realizations, are indicated by markers 'o'. As a reference, we have also included corresponding performance results for i.i.d. Rayleigh–fading ($L\in\{1,...,4\}$). As can be seen, the relative performance gains obtained for $L>1$ diversity branches are quite similar for double Rayleigh fading and conventional Rayleigh fading. However, in comparison the BEP performance for double Rayleigh fading is significantly worse than that for Rayleigh fading (for all values of L).[12] For example, in the case of $L=4$ diversity branches, the performance difference between double Rayleigh fading and conventional Rayleigh fading at a BEP of 10^{-4} is about 5.3 dB. Vice versa, in order to achieve a BEP of less than $3\cdot10^{-4}$ at a (normalized) overall SNR of 20 dB, one requires $L=4$ diversity branches in the case of double Rayleigh fading, whereas in the case of conventional Rayleigh fading $L=2$ diversity branches are sufficient. Finally, we note that the analytical results and the simulation results are in good agreement, which corroborates our analysis in Section III-A.

In Fig. 2, the average BEP $\bar{P}_{\mathrm{b}}(\theta)$ for binary DPSK modulation with EGC at the receiver is compared to that of coherent binary PSK modulation with MRC at the receiver. As an example, we consider again the case of i.i.d. double Rayleigh fading ($k=1$, $m=1$). The analytical curves for binary PSK modulation were obtained based on (14) and (46) using numerical integration. As can be seen, the general behavior of the curves for growing values of L is quite similar in the case of binary DPSK and binary PSK modulation. In particular, the asymptotic slopes of the curves are identical in both cases, as predicted by our asymptotic analysis in Section IV-A. Interestingly, the performance difference between binary DPSK and binary PSK modulation at high SNR values is about 3.8 dB (for all values of L), which is slightly larger than the well–known 3 dB difference in the case of conventional Rayleigh fading.

Finally, Fig. 3 compares the average BEP $\bar{P}_{\mathrm{b}}(\theta)$ of binary DPSK with EGC at the receiver for various examples of i.i.d. cascade Rayleigh/Nakagami–m fading ($k=1$, $m\in\{1,3,5\}$, $L\in\{1,3\}$). For the example $m=3$, we have also included the average BEP of coherent binary PSK modulation with MRC at the receiver. Moreover, for the example $m=3$, $L=3$ we have included the asymptotic BEP curves as a reference (dotted lines), which were evaluated based on (38) and (47) for binary DPSK and binary PSK modulation, respectively. As can be seen, the performance of binary DPSK improves significantly, if the fading parameter m is increased from $m=1$ to $m=3$. As opposed to this, increasing m further to $m=5$ yields comparatively small additional performance gains, which indicates that the BEP performance is somewhat limited by the small value of the fading parameter k. For the case $L=1$, this can also be seen from (6). The AF expression is clearly dominated by the smaller of the two parameters k and m, which is in accordance with our findings concerning the resulting diversity order (Section IV-A). In the considered example, the AF expression is dominated by parameter k (due to the term $1/k$). Correspondingly, an increase of m from $m=3$ to $m=5$, which reduces the AF from 1.667 to 1.4, yields only small performance improvements in this example.

Another interesting observation from Fig. 3 is that the performance difference between binary DPSK and binary PSK modulation at high SNR values is slightly reduced if the fading pa-

[12] For the special case $L=1$ and coherent PSK modulation, this observation was already made in [4].

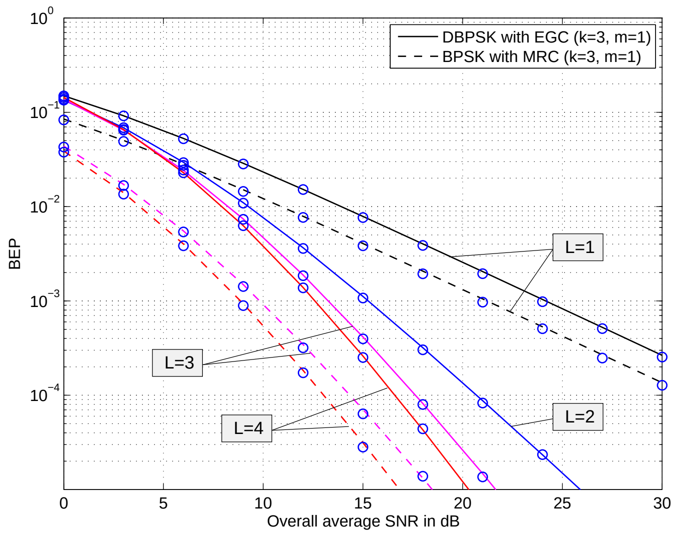

Fig. 4. Average BEP $\bar{P}_{\rm b}(\theta)$ versus (normalized) overall average SNR $L\,\theta$ in dB for the case $k = 3$ and $m = 1$ (mild shadowing). Solid lines represent analytical results for DBPSK modulation with EGC at the receiver evaluated based on (34) using the values $k=3.01$ and $m=0.99$. Dashed lines represent corresponding analytical results for coherent BPSK modulation with MRC at the receiver evaluated based on (19), (46) using numerical integration. Corresponding simulation results for $k=3$ and $m=1$ are indicated by markers 'o' (both for DPSK and PSK modulation).

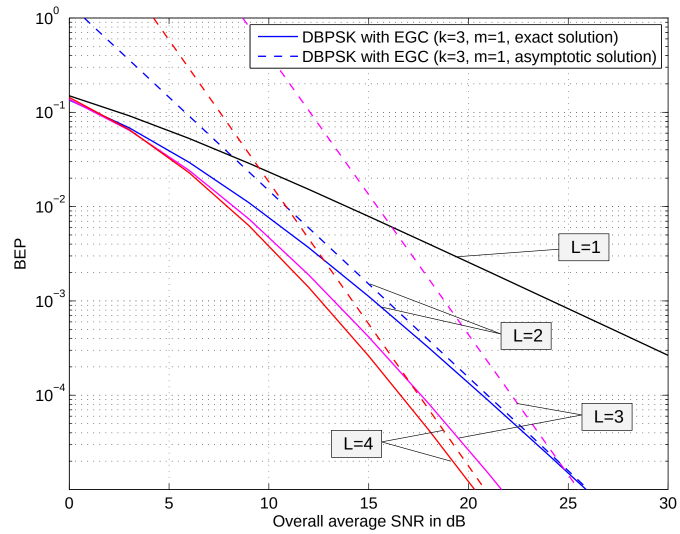

Fig. 5. Average BEP $\bar{P}_{\rm b}(\theta)$ versus (normalized) overall average SNR $L\,\theta$ in dB for the case $k = 3$ and $m = 1$ (mild shadowing). Solid lines represent analytical results for DBPSK modulation with EGC at the receiver, evaluated based on (34) using the values $k=3.01$ and $m=0.99$. Dashed lines represent corresponding asymptotic results evaluated based on (50).

rameter m is increased. For example, in the case $m=3$ the performance difference is about 3.3 dB, as opposed to 3.8 dB in the case of double Rayleigh fading, cf. Fig. 2. Finally, we again note that the analytical results (evaluated based on (27) and (28) using the values $k=1.01$ and $m\in\{0.99,\,2.99,\,4.99\}$) and the simulation results for $k=1$ and $m\in\{1,3,5\}$ are in good agreement for all considered cases. Moreover, the asymptotic BEP curves accurately represent the behavior at high SNR values, which corroborates our asymptotic analysis in Section IV-A.

B. Correlated Composite Shadowing and Multipath Fading

Next, we consider the BEP performance of binary DPSK modulation over L diversity branches that are subject to correlated composite shadowing and multipath fading (cf. Section III-B and IV-B). Fig. 4 presents numerical results for the average BEP $\bar{P}_{\rm b}(\theta)$ as a function of the normalized overall average received SNR $L\,\theta$ in dB for the case $k=3$ and $m=1$ (mild shadowing) and $L\in\{1,\ldots,4\}$. Solid lines represent analytical results evaluated based on (34), using the values $k=3.01$ and $m=0.99$. Dashed lines represent analytical results for coherent binary PSK modulation with MRC at the receiver (for the cases $L\in\{1,3,4\}$), evaluated based on (19) and (46) using the same values $k=3.01$ and $m=0.99$. Corresponding simulation results for $k=3$ and $m=1$, obtained by Monte–Carlo simulations over a large number of independent channel realizations, are indicated by markers 'o' (both for DPSK and PSK modulation). As can be seen, the analytical results and the simulation results are in good agreement, which corroborates our analysis in Section III-B. Note that significant diversity gains are accomplished in the case $L>1$, both in the case of DPSK and PSK modulation. As can be seen, the general behavior of the BEP curves is the same for coherent and non–coherent transmission (similar to the case of i.i.d. cascade Rayleigh/Nakagami–m fading). The asymptotic advantage of binary PSK over binary DPSK modulation is about 3 dB, similar to the case of pure Rayleigh fading.

In Fig. 5, we compare the exact analytical BEPs for DPSK modulation according to (34) with the asymptotic BEPs according to (50).[13] As earlier, the values $k=3.01$ and $m=0.99$ were employed for evaluating the expressions (34) and (50). It can be seen that convergence is comparatively fast for the cases $L=2$ and $L=4$. In particular, the BEP curves exhibit the predicted diversity orders of $d = 2m = 2$ and $d = k = 3$, respectively. However, as discussed in Section IV-B, in the case $L=3$ convergence is very slow, since $k \approx mL$. In this example, (normalized) SNR values on the order of 100 dB are required, until the exact analytical BEP (34) approaches the asymptotic BEP (50) and assumes the predicted asymptotic diversity order of $d\!=\!3m\!\approx\!k\!\approx\!3$. Note that since the maximum diversity order is accomplished for $L=3$, the relative performance advantage of $L>3$ branches is comparatively small in this example.

Finally, in Fig. 6 numerical performance results for the case $k=1$ and $m=3$ (moderate shadowing) and $L\in\{1,4\}$ are presented. Again it can be seen that the analytical results (solid lines for binary DPSK and dashed lines for binary PSK modulation) and the simulation results (markers 'o') are in good agreement. The analytical results for binary DPSK and binary PSK modulation were again evaluated based on (34) and (19), (46), respectively, using the values $k=1.01$ and $m=2.99$. Interestingly, in contrast to the case of mild shadowing, in this example $L>1$ branches offer no diversity benefit at all. As can be seen, in the case of binary DPSK modulation the BEP curve for $L=4$ is even slightly worse than the BEP curve for

[13] For binary PSK modulation with MRC at the receiver we have obtained very similar results (not depicted) by evaluating asymptotic BEPs according to (53) and comparing them with the corresponding analytical BEPs according to (19) and (46).

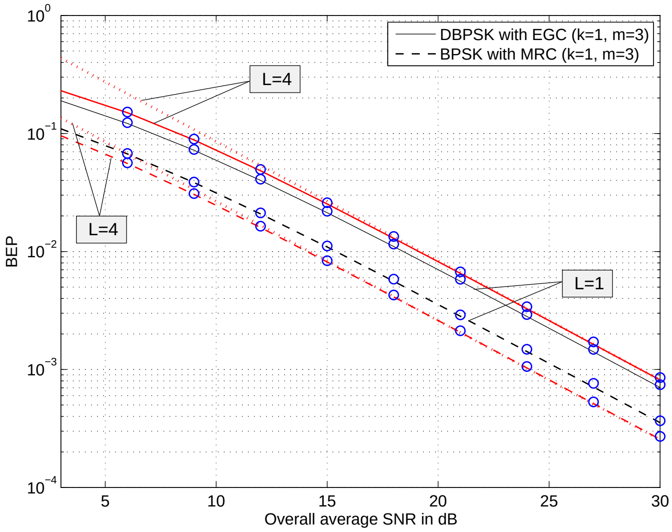

Fig. 6. Average BEP $\bar{P}_\mathrm{b}(\theta)$ versus (normalized) overall average SNR $L\,\theta$ in dB for the case $k=1$ and $m=3$ (moderate shadowing). Solid lines represent analytical results for DBPSK modulation with EGC at the receiver evaluated based on (34) using the values $k=1.01$ and $m=2.99$. Dashed lines represent corresponding analytical results for coherent BPSK modulation with MRC at the receiver evaluated based on (19), (46) using numerical integration. Corresponding simulation results for $k=1$ and $m=3$ are indicated by markers 'o' (both for DPSK and PSK modulation). The dotted lines represent asymptotic BEP curves for the case $L=4$ evaluated based on (50) for DPSK modulation and based on (53) for PSK modulation.

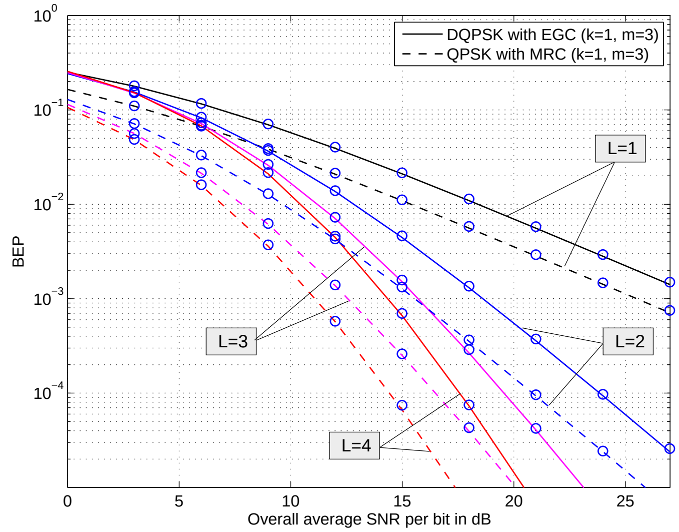

Fig. 7. Average BEP $\bar{P}_\mathrm{b}(\theta)$ versus (normalized) overall average SNR per bit $L\,\theta/2$ in dB for the case of cascade fading with $k=1$ and $m=3$. Solid lines represent analytical results for quaternary DPSK (DQPSK) modulation with EGC at the receiver evaluated based on (14) and (55) using the values $k=1.01$ and $m=2.99$. Dashed lines represent corresponding analytical results for coherent quaternary PSK (QPSK) modulation with MRC at the receiver evaluated based on (14) and (46) using numerical integration. Corresponding simulation results for $k=1$ and $m=3$ are indicated by markers 'o' (both for DPSK and PSK modulation).

$L=1$ (since due to the SNR normalization the average branch SNR scales with $1/L$). The BEP curves for $L=2$ and $L=3$ (not depicted) lie in between the curves for $L=1$ and $L=4$. As predicted by the asymptotic BEP (50), included here for the case $L=4$ (dotted line), the BEP curves of binary DPSK for $L\geq 1$ branches are all characterized by the same asymptotic diversity order of $d=k=1$. Also note that the convergence of the asymptotic BEP (50) to the exact BEP (34) is comparatively fast in this example. Moreover, we note that while in the case of binary PSK modulation the asymptotic diversity order is the same as for binary DPSK modulation, the order of the curves is swapped here, i.e., $L=4$ offers a slight performance advantage over $L=1$ (the BEP curves for $L=2$ and $L=3$ were again found in between the curves for $L=1$ and $L=4$). Finally, we note that in the case of severe shadowing (not depicted), the BEP curves were found to exhibit a very similar behavior to that in Fig. 6. For example, for $k=0.5$ and $m=3$ we found that the curves for $L=1$ to $L=4$ are similarly close as in Fig. 6 (both for binary DPSK and for binary PSK modulation) and that the relative performance of binary DPSK and for binary PSK modulation is comparable. Moreover, we again found that increasing the number of diversity branches leads to slight performance improvements in the case of binary PSK and to slight performance degradations in the case of binary PSK modulation. The main difference compared to the case $k=1$ is that for $k=0.5$ the BEP curves exhibit a reduced diversity order of 0.5 for all $L\in\{1,\ldots,4\}$ (as expected), which leads to significant performance degradations for all curves.

The above behavior in the presence of moderate or severe shadowing can again be illustrated by considering the corresponding AF expression [12]:

$$\mathrm{AF} = \frac{1}{k}+\frac{1}{mL}+\frac{1}{kmL}. \tag{65}$$

As can be seen, in the case of moderate or severe shadowing ($k\leq 1$), the AF expression is clearly dominated by parameter k, which explains why increasing the number of diversity branches, L, does not offer any notable performance improvements in the above examples. For example, if $k=0.5$, increasing the number of diversity branches from $L=1$ to $L=4$ reduces the AF from 3 to 2.25, which is still a significant value compared, e.g., to Rayleigh fading ($\mathrm{AF}=1$). This finding implies that one would require macroscopic diversity (e.g., through spatially separated antennas) in addition to microscopic diversity, in order to overcome the effects of shadowing. This issue has been addressed in [17], based on a partially correlated generalized K–fading model. Note that the limiting case of uncorrelated shadowing is already covered by our results on i.n.d. generalized K–fading, although we have related this case to a cascade–fading scenario throughout this paper.

C. Performance of M–ary Modulation Schemes

Finally, we present some numerical performance results for M–ary modulation. As an example, we focus on the case of quaternary DPSK and coherent quaternary PSK modulation over L i.i.d. cascade Rayleigh/Nakagami–m fading branches with $k=1$ and $m=3$. Fig. 7 displays the corresponding average BEPs $\bar{P}_\mathrm{b}(\theta)$ versus the normalized overall average received SNR per bit $L\,\theta/2$ in dB for $L\in\{1,\ldots,4\}$ diversity branches. The analytical results for quaternary DPSK modulation with EGC at the receiver (solid lines) were evaluated based on (14) and (55) via numerical integration using the values $k = 1.01$ and $m = 2.99$. The analytical results for coherent quaternary PSK modulation with MRC at the receiver (dashed lines) were evaluated based on (14) and (46), exploiting the fact that the average BEP of quaternary PSK with Gray mapping is identical to that of binary PSK modulation. As can be seen, the basic behavior of the BEP curves is very similar to the case of binary DPSK/PSK modulation.[14] In particular, the asymptotic slope of the BEP curves as well as the performance difference between quaternary DPSK and quaternary PSK modulation is the same as in the case of binary transmission (cf. Fig. 3). Again, we note that the analytical results and the simulation results are in good agreement, which corroborates our analysis in Section V.

VII. CONCLUSIONS

The generalized K–fading model, which is characterized by two fading parameters, $k>0$ and $m>0$, is versatile enough to cover both scenarios with cascade multipath fading and scenarios with composite shadowing and multipath fading. In this paper, we have derived closed–form expressions for the BEP of binary DPSK modulation and binary non–coherent FSK modulation over L generalized K–fading links. In particular, we have considered the case of independent fading across links, which is relevant for cascade multipath fading scenarios, and the case of correlated composite shadowing and multipath fading. Moreover, we have conducted an asymptotic performance analysis for high SNR values and have studied the resulting diversity orders for various cases. We have also discussed the extension of our results to M–ary modulation schemes.

Our results have shown that there is an interesting interplay between the two fading parameters k and m. In the case of independent fading, the smaller of the two fading parameters limits the asymptotic diversity order. Similarly, in the case of correlated composite shadowing and multipath fading, the asymptotic diversity order is always limited by either the shadowing effect or the multipath fading, depending on which one of the two fading effects is more severe. Moreover, for both scenarios we have shown that the diversity order of the considered non–coherent transmission schemes is, in fact, the same as in the case of a coherent transmission scheme. Finally, numerical performance results were presented, in order to illustrate the above findings, and our analytical performance results were corroborated by means of Monte–Carlo simulations.

REFERENCES

[1] D. Tse and P. Viswanath, *Fundamentals of Wireless Communication*. New York: Cambridge University Press, 2005.

[2] P. M. Shankar, "Error rates in generalized shadowed fading channels," *Wireless Personal Commun.*, vol. 28, no. 4, pp. 233–238, Feb. 2004.

[3] V. Erceg, S. J. Fortune, J. Ling, A. J. Rustako, Jr., and R. A. Valenzuela, "Comparisons of a computer–based propagation prediction tool with experimental data collected in urban microcellular environments," *IEEE J. Selected Areas Commun.*, vol. 15, no. 4, pp. 677–684, May 1997.

[4] J. Salo, H. M. El–Sallabi, and P. Vainikainen, "Impact of double–Rayleigh fading on system performance," in *Proc. Int. Symp. on Wireless Pervasive Computing (ISWPC)*, Phuket, Thailand, Jan. 2006.

[5] H. G. Sandalidis, T. A. Tsiftsis, G. K. Karagiannidis, and M. Uysal, "BER performance of FSO links over strong atmospheric turbulence channels with pointing errors," *IEEE Commun. Lett.*, vol. 12, no. 1, pp. 44–46, Jan. 2008.

[14] We have made the same observation for the case of correlated composite shadowing and multipath fading (not depicted).

[6] E. Bayaki, R. Schober, and R. K. Mallik, "Performance analysis of free–space optical systems in Gamma–Gamma fading," in *Proc. IEEE Global Commun. Conf. (Globecom'08)*, New Orleans, LA, Dec. 2008.

[7] N. D. Chatzidiamantis and G. K. Karagiannidis, "On the distribution of the sum of Gamma–Gamma variates and applications in RF and optical wireless communications," submitted to *IEEE Trans. Commun.*, May 2009 (Online: http://arxiv.org/abs/0905.1305v1).

[8] M. Niu, J. Cheng, J. F. Holzman, and L. McPhail, "Performance analysis of coherent free space optical communication systems with K–distributed turbulence," in *Proc. IEEE Int. Conf. Commun. (ICC'09)*, Dresden, Germany, June 2009.

[9] A. Abdi and M. Kaveh, "Comparison of DPSK and MSK bit error rates for K and Rayleigh–lognormal fading distributions," *IEEE Commun. Lett.*, vol. 4, no. 4, pp. 122–124, Apr. 2000.

[10] A. Abdi, H. A. Barger, and M. Kaveh, "A simple alternative to the lognormal model of shadow fading in terrestrial and satellite channels," in *Proc. IEEE Veh. Technol. Conf. (VTC'01)*, Atlantic City, NJ, Oct. 2001, pp. 2058-2062.

[11] I. M. Kostić, "Analytical approach to performance analysis for channel subject to shadowing and fading," *IET Proc. Commun.*, vol. 152, no. 6, pp. 821–827, Dec. 2005.

[12] P. M. Shankar, "Performance analysis of diversity combining algorithms in shadowed fading channels," *Wireless Personal Commun.*, vol. 37, no. 1–2, pp. 61–72, Apr. 2006.

[13] P. S. Bithas, N. C. Sagias, P. T. Mathiopoulos, G. K. Karagiannidis, and A. A. Rontogiannis, "On the performance analysis of digital communications over generalized–K fading channels," *IEEE Commun. Lett.*, vol. 10, no. 5, pp. 353–355, May 2006.

[14] P. S. Bithas, P. T. Mathiopoulos, and S. A. Kotsopoulos, "Diversity reception over generalized–K (K_G) fading channels," *IEEE Trans. Wireless Commun.*, vol. 6, no. 12, pp. 4238-4243, Dec. 2007.

[15] A. Laourine, M.–S. Alouini, S. Affes, and A. Stéphenne, "On the capacity of generalized–$\mathcal{K}$ fading channels," *IEEE Trans. Wireless Commun.*, vol. 7, no. 7, pp. 2441–2445, July 2008.

[16] P. S. Bithas, N. C. Sagias, P. T. Mathiopoulos, S. A. Kotsopoulos, and A. M. Maras, "On the correlated K–distribution with arbitrary fading parameters," *IEEE Signal Processing Lett.*, vol. 15, pp. 541–544, 2008.

[17] P. M. Shankar, "Macrodiversity and microdiversity in correlated shadowed fading channels," *IEEE Trans. Veh. Technol.*, vol. 58, no. 2, pp. 727–732, Feb. 2009.

[18] I. Trigui, A. Laourine, S. Affes, and A. Stéphenne, "Outage analysis of wireless systems over composite fading/shadowing channels with co–channel interference," in *Proc. IEEE Wireless Commun. & Networking Conf. (WCNC'09)*, Budapest, Hungary, Apr. 2009.

[19] M. Uysal, "Diversity analysis of space–time coding in cascaded Rayleigh fading channels," *IEEE Commun. Lett.*, vol. 10, no. 3, pp. 165–167, Mar. 2006.

[20] N. H. Tran, H. H. Nguyen, and T. Le–Ngoc, "Application of signal space diversity in BICM–ID over cascaded Rayleigh fading channels," in *Proc. IEEE Int. Conf. Commun. (ICC'07)*, Glasgow, Scotland, June 2007, pp. 4011–4016.

[21] M. K. Simon and M. S. Alouini, *Digital Communication Over Fading Channels*, 2nd ed. Hoboken, NJ: John Wiley & Sons, 2005.

[22] M. Nakagami, "The m distribution: a general formula for intensity distribution of rapid fading," in W. C. Hoffman (Ed.) *Statistical Methods in Radio Wave Propagation*, Pergamon: New York, 1960.

[23] I. S. Gradsheteyn and I. M. Ryzhik, *Table of Integrals, Series, and Products*, 7th ed. New York, NY: Academic Press, 1994.

[24] M. Abramowitz and I. A. Stegun (Eds.), *Handbook of Mathematical Functions*, 10th ed. Washington, D. C.: National Bureau of Standards, 1972.

[25] Wolfram Mathworld, 2009 [Online]: http://functions.wolfram.com/HypergeometricFunctions/HypergeometricU/27/01/

[26] Wolfram Mathworld, 2009 [Online]: http://functions.wolfram.com/HypergeometricFunctions/LaguerreL3General/26/01/02/

[27] J. G. Proakis, *Digital Communications*, 4th ed. New York, NY: McGraw–Hill, 2001.

[28] Wolfram Mathworld, 2009 [Online]: http://functions.wolfram.com/HypergeometricFunctions/HypergeometricU/06/01/03/01/

[29] M.–S. Alouini and A. J. Goldsmith, "A unified approach for calculating error rates of linearly modulated signals over generalized fading channels," *IEEE Trans. Commun.*, vol. 47, no. 9, pp. 1324–1334, Sept. 1999.

[30] G. Arfken, *Mathematical Methods for Physicists*, 3rd ed. Orlando, FL: Academic Press, 1985.

[31] Wolfram Mathworld, 2009 [Online]: http://functions.wolfram.com/HypergeometricFunctions/LaguerreL3General/06/01/03/01/01/

APPENDIX

In the following, we prove the validity of (63) for the case of fully correlated shadowing/i.i.d. multipath fading, by extending the derivation of (55) presented in [21, Ch. 9.4] accordingly.

Given a fixed value of the instantaneous EGC output SNR γ_{t}, the BEP of quaternary DPSK modulation with Gray mapping over L branches with EGC at the receiver can be written as

$$\bar{P}_{\mathrm{b}}(\gamma_{\mathrm{t}}) = \frac{1}{\pi\, 2^{2L}} \int_{-\pi}^{\pi} \frac{f(L,\rho;\phi)}{1+2\rho\sin(\phi)+\rho^2} \times \prod_{l=1}^{L} \exp\left(-\frac{b^2\gamma_l}{2}\left(1+2\rho\sin(\phi)+\rho^2\right)\right) \mathrm{d}\phi, \quad (66)$$

where $f(L,\rho;\phi)$ and ρ are given by (56) and (60), respectively, and $b \triangleq \sqrt{2+\sqrt{2}}$ [21, Ch. 9.4]. The average BEP $\bar{P}_{\mathrm{b}}(\theta)$ can thus be written as

$$\bar{P}_{\mathrm{b}}(\theta) = \int_0^{\infty} \cdots \int_0^{\infty} \bar{P}_{\mathrm{b}}(\gamma_{\mathrm{t}}) \int_0^{\infty} \prod_{l=1}^{L} p_{\gamma_l|\bar{\gamma}}(\gamma_l|\bar{\gamma}) \times\; p_{\bar{\gamma}}(\bar{\gamma})\, \mathrm{d}\bar{\gamma}\; \mathrm{d}\gamma_1 \cdots \gamma_L, \quad (67)$$

where we have used that the joint PDF $p_{\gamma_1,\ldots,\gamma_L|\bar{\gamma}}(\gamma_1,\ldots,\gamma_L|\bar{\gamma})$, conditioned on the average SNR $\bar{\gamma}$, can be written as the product of the conditional PDFs $p_{\gamma_l|\bar{\gamma}}(\gamma_l|\bar{\gamma})$ of the instantaneous branch SNRs γ_l ($l \in \{1,\ldots,L\}$), cf. (15). Using (66) one obtains

$$\begin{aligned}
\bar{P}_{\mathrm{b}}(\theta) &= \frac{1}{\pi\, 2^{2L}} \int_{-\pi}^{\pi} \frac{f(L,\rho;\phi)}{1+2\rho\sin(\phi)+\rho^2} \quad (68)\\
&\times \int_0^{\infty} \left[\prod_{l=1}^{L} \int_0^{\infty} \exp\left(-\frac{b^2\gamma_l}{2}\left(1+2\rho\sin(\phi)+\rho^2\right)\right) \times\; p_{\gamma_l|\bar{\gamma}}(\gamma_l|\bar{\gamma})\, \mathrm{d}\gamma_l\right] p_{\bar{\gamma}}(\bar{\gamma})\, \mathrm{d}\bar{\gamma}\;\; \mathrm{d}\phi\\
&= \frac{1}{\pi\, 2^{2L}} \int_{-\pi}^{\pi} \frac{f(L,\rho;\phi)}{1+2\rho\sin(\phi)+\rho^2}\\
&\times \int_0^{\infty} \left[\mathrm{M}_{\gamma_l|\bar{\gamma}}\left(-\frac{b^2}{2}\left(1+2\rho\sin(\phi)+\rho^2\right)\right)\right]^L \times p_{\bar{\gamma}}(\bar{\gamma})\, \mathrm{d}\bar{\gamma}\;\; \mathrm{d}\phi\\
&= \frac{1}{\pi\, 2^{2L}} \int_{-\pi}^{\pi} \frac{f(L,\rho;\phi)}{1+2\rho\sin(\phi)+\rho^2} \times \mathrm{M}_{\gamma_{\mathrm{t}}}\left(-\frac{b^2}{2}\left(1+2\rho\sin(\phi)+\rho^2\right)\right) \mathrm{d}\phi,
\end{aligned}$$

where we have used that the multipath fading is i.i.d., i.e., the conditional MGFs $\mathrm{M}_{\gamma_l|\bar{\gamma}}(x)$ are identical for all branches $l \in \{1,\ldots,L\}$ and the (unconditional) MGF $\mathrm{M}_{\gamma_{\mathrm{t}}}(x)$ is given by $\mathrm{M}_{\gamma_{\mathrm{t}}}(x) = \int_0^{\infty} [\mathrm{M}_{\gamma_l|\bar{\gamma}}(x)]^L\, p_{\bar{\gamma}}(\bar{\gamma})\, \mathrm{d}\bar{\gamma}$. Combining (68) with the values for ρ and b, one finally arrives at (63). $\square$

Cindy Zhu (S'07) was born in Shenyang, China, in 1984. She received the B.A.Sc. and the M.A.Sc. degrees in Electrical Engineering from the University of British Columbia, Vancouver, Canada, in 2007 and 2009, respectively. Her research interests concern wireless communication systems, in particular non-coherent detectors and the generalized K-fading model.

Jan Mietzner (S'02, M'08) was born in Rendsburg, Germany, on March 6, 1975. He studied electrical engineering and information engineering at the Faculty of Engineering, Christian-Albrechts University (CAU) of Kiel, Germany, with focus on digital communications. During his studies, he spent six months in 2000 with the Global Wireless Systems Research Group, Lucent Technologies, Bell Labs U.K., in Swindon, England. He received the Dipl.-Ing. degree from the CAU Kiel in July 2001. For his diploma thesis on space-time codes he received the Prof.-Dr.- Werner-Petersen Award. From August 2001 to October 2006 he was working toward his Ph.D. degree as a research and teaching assistant at the Information and Coding Theory Lab (ICT), Faculty of Engineering, CAU Kiel, and received his Ph.D. degree in December 2006. He received an award from the Friends of the Faculty of Engineering for the best dissertation in 2006. From January 2007 to December 2008 he was with the Communication Theory Group, Department of Electrical and Computer Engineering, University of British Columbia, in Vancouver, Canada, as a post-doctoral research fellow sponsored by the German Academic Exchange Service (DAAD). His research interests concern physical layer aspects of future wireless communication systems, especially multiple-antenna techniques, ultra-wideband (UWB) and cognitive radio systems, relaying, and cooperative diversity techniques. Dr. Mietzner has served as a TPC member for the IEEE WCNC 2009 & 2010 and the IEEE Globecom 2009. In March 2009, he joined EADS Germany, Defence & Security, in Ulm, Germany.

Robert Schober (S'98, M'01, SM'08, F'10) was born in Neuendettelsau, Germany, in 1971. He received the Diplom (Univ.) and the Ph.D. degrees in electrical engineering from the University of Erlangen-Nuremberg in 1997 and 2000, respectively. From May 2001 to April 2002 he was a Postdoctoral Fellow at the University of Toronto, Canada, sponsored by the German Academic Exchange Service (DAAD). Since May 2002 he has been with the University of British Columbia (UBC), Vancouver, Canada, where he is now a Full Professor and Canada Research Chair (Tier II) in Wireless Communications. His research interests fall into the broad areas of Communication Theory, Wireless Communications, and Statistical Signal Processing. Dr. Schober received the 2002 Heinz MaierLeibnitz Award of the German Science Foundation (DFG), the 2004 Innovations Award of the Vodafone Foundation for Research in Mobile Communications, the 2006 UBC Killam Research Prize, the 2007 Wilhelm Friedrich Bessel Research Award of the Alexander von Humboldt Foundation, and the 2008 Charles McDowell Award for Excellence in Research from UBC. In addition, he received best paper awards from the German Information Technology Society (ITG), the European Association for Signal, Speech and Image Processing (EURASIP), IEEE ICUWB 2006, the International Zurich Seminar on Broadband Communications, and European Wireless 2000. Dr. Schober is also the Area Editor for Modulation and Signal Design for the IEEE Transactions on Communications.